Plant KASH proteins SINE1 and SINE2 have synergistic and antagonistic interactions with actin branching and actin bundling factors.

Morgan Moser[1#], Norman R. Groves[1,3], and Iris Meier[1,2,3*]

[1]Department of Molecular Genetics, The Ohio State University, Columbus, OH, USA

[2] Center for RNA Biology, The Ohio State University, Columbus, OH, USA

[3]Center for Applied Plant Sciences, The Ohio State University, Columbus, OH, USA

* Address correspondence to meier.56@osu.edu

Current address: Institute of Genomic Medicine, Nationwide Children's Hospital, Columbus, OH

Research Highlight: The plant KASH proteins SINE1 and SINE2, components of LINC complexes, genetically interact with the actin remodeling factor SCAB1 and the ARP2/3 complex in stomatal dynamics and plant development.

Abstract

Linker of nucleoskeleton and cytoskeleton complexes consist of outer nuclear membrane KASH proteins, interacting in the nuclear envelope lumen with inner nuclear membrane SUN proteins and connecting nucleus and cytoskeleton. The paralogous Arabidopsis KASH proteins SINE1 and SINE2 function during stomatal dynamics induced by light-dark transitions and ABA, which requires F-actin reorganization. SINE2 influences actin depolymerization and SINE1 actin repolymerization. The actin-related protein 2/3 (ARP2/3) complex, an actin nucleator, and the plant actin bundling and stabilizing factor SCAB1 are involved in stomatal aperture control. Here, we have tested the genetic interaction of SINE1 and SINE2 with SCAB1 and the ARP2/3 complex. We show that SINE1 and the ARP2/3 complex function in the same pathway during ABA-induced stomatal closure, while SINE2 and the ARP2/3 complex play opposing roles. The actin repolymerization defect observed in *sine1-1* is partially rescued in *scab1-2 sine1-1,* while *SINE2* is epistatic to *SCAB1*. In addition, SINE1 and ARP2/3 act synergistically in lateral root development. Absence of SINE2 renders trichome development independent of the ARP2/3 complex. Together, these data reveal complex and differential interactions of the two KASH proteins with the actin-remodeling apparatus and add evidence to the proposed differential role of SINE1 and SINE2 in actin dynamics.

Keywords: Actin, ARP2/3 Complex, Cytoskeleton, Guard Cells, LINC Complex, KASH, Stomata, Trichomes

Introduction

Arabidopsis SUN-interacting nuclear envelope protein 1 and 2 (SINE1 and SINE2) are components of a plant Linker of Nucleoskeleton and Cytoskeleton (LINC) complex. LINC complexes are protein complexes that span both the outer nuclear membrane (ONM) and inner nuclear membrane (INM) through binding between the ONM Klarsicht/ANC-1/Syne Homology (KASH) proteins, and the INM Sad1/Unc-84 (SUN) proteins (Starr and Fridolfsson, 2010; Meier et al., 2017). SINE1 and SINE2 are paralogous plant KASH proteins that bind to Arabidopsis SUN1 and SUN2 and are conserved among land plants (Zhou et al., 2014; Poulet et al., 2017). Both proteins have an N-terminal domain with homology to the armadillo repeat (ARM) domain (Coates, 2003), and the SINE1 ARM domain colocalizes with filamentous actin (F-actin) (Zhou et al., 2014).While Arabidopsis SINE1 and SINE2 are both expressed in roots, in leaves SINE1 is expressed only in the stomatal lineage while SINE2 is expressed in trichomes, epidermal and mesophyll cells, and weakly in mature guard cells (Zhou et al., 2014).

We have previously shown that loss of SINE1 or SINE2 results in impaired stomatal closure in response to ABA and dark (Biel et al., 2020a). This defect is, in part, attributed to impairments in F-actin reorganization (Biel et al., 2020a; Biel et al., 2022). In WT stomata, F-actin is radially arrayed in open guard cells, and upon the onset of closure, F-actin depolymerizes and is reorganized into a linear, bundled array (Li et al., 2012). Disruption of this reorganization, for example by actin-depolymerizing drugs, perturbs stomatal dynamics (Jiang et al., 2012; Kim et al., 1995; Li et al., 2014; Xiao et al., 2004; Zhao et al., 2016). SINE1 and SINE2 appear to regulate different stages of actin reorganization, with SINE2 required for early actin

depolymerization and SINE1 for later actin filament and bundle reassembly (Biel et al., 2022). It is currently not known how these activities of SINE1 and SINE2 relate to their localization at the nuclear envelope or to the fact that the ARM domain of SINE1 co-localizes with F-actin while the ARM domain of SINE2 does not. Loss of SINE1 or SINE2 also results in disrupted microtubule reorganization during ABA-induced stomatal closure (Biel et al., 2020b).

The actin-nucleating complex ARP2/3 and the plant-specific actin-stabilizing protein SCAB1 are also required for actin reorganization during ABA-induced stomatal closure. The ARP2/3 complex functions in F-actin nucleation and branching, where the new daughter filament is extended from an existing mother filament in a y-branch configuration (Goley and Welch, 2006). The complex is composed of seven distinct subunits, which include the actin-related proteins (ARP) ARP2 and ARP3 and the additional ARP2/3 complex (ARPC) proteins ARPC1-ARPC5 (Goley et al., 2010). Four of the seven subunits have specific functions, with ARP2 and ARP3 acting as a template for daughter filament nucleation (functioning as an actin-like heterodimer), while ARPC2 and ARPC4 form the interface that binds to the mother actin filament for branching (Gournier et al., 2001). Disruption of ARP2/3 complex function and regulation in Arabidopsis results in distorted trichomes and reduced pavement cell lobing (Mathur et al., 2003a; Mathur et al., 2003b; Ivakov and Persson, 2013; Sahi et al., 2018). Mutants also exhibit altered microtubule organization and changes in cell wall composition (Saedler et al., 2004; Zhang et al., 2005; Sahi et al., 2018). The ARP2/3 complex is important for stomatal dynamics, specifically with actin filament reorganization during opening and closing (Jiang et al., 2012; Li et al., 2012; Li et al., 2014). In mutants lacking one subunit of the ARP2/3 complex, actin filament organization is disrupted, and stomatal closure is perturbed (Jiang et al., 2012; Li et al., 2014).

SCAB1 is a plant-specific actin-binding protein that can stabilize and bundle actin filaments and is predominantly expressed in guard cells (Winter et al., 2007; Zhao et al., 2011). Overexpression or loss of SCAB1 results in impaired ABA-induced stomatal closure associated with increased and decreased F-actin stability, respectively (Zhao et al., 2011). SCAB1 activity is regulated by the signaling molecule phosphatidylinositol 3-phosphate (PI3P) (Yang et al., 2021).

Here, we tested genetic interactions between SINE1 and SINE2 and ARP2/3 and/or SCAB1 in the context of stomatal dynamics and actin reorganization during ABA-induced guard cell closure. In addition, we report genetic interactions between SINE1 and SINE2 and the ARP2/3 complex for additional aspects of plant growth and development.

Materials and Methods

Plant material and growth

Arabidopsis thaliana (Columbia-0 ecotype) was germinated on Murashige and Skoog medium plates (Caisson Laboratories) containing 1% sucrose under constant light. Plants at the two-leaf stage were transplanted to soil and grown at an average temperature of 22-23°C and grown under a 16-hour light/8-hour dark or 8-hour light/16-hour dark regime. *sine1-1* (SALK_018239C; Zhou et al., 2014), *sine2-1* (CS801355; Zhou et al., 2014), *arpc4-1* (SALK_073297C; Kotchoni et al., 2009), and *scab1-2* (SAIL_193_E09; Zhao et al., 2011) were obtained from the Arabidopsis Biological Resource Center. Crosses were performed between *sine1-1* or *sine2-1* and *arpc4-1* or *scab1-2* to create the double mutants *arcp4-1 sine1-1*, *arpc4-1 sine2-1*, *scab1-2 sine1-1*, and *scab1-2 sine2-1*.

GFP-LIFEACT-expressing *sine1-1* and *sine2-1* lines were previously reported (Biel et al., 2022). Double mutant lines expressing 35Spro::GFP-LIFEACT were generated by crossing GFP-LIFEACT *sine1-1* or *sine2-1* with the corresponding double mutants (*arcp4-1 sine1-1* or *scab1-2 sine1-1* for *sine1-1*; *sine2-1* or *scab1-2 sine2-1* for *sine2-1*). In addition, the previously reported *sine1-1 sine2-1* double mutant (Biel et al., 2020a) was crossed with the same GFP-LIFEACT line as above to generate GFP-LIFEACT-expressing *sine1-1 sine2-1*. F2 lines homozygous for the T-DNA insertions and hemizygous or homozygous for GFP-LIFEACT were used for confocal imaging.

Stomatal aperture measurements

Stomatal closing assays were performed using rosette leaves of 6-8 week-old plants grown under short-day conditions (8 hours light; 16 hours dark). Leaves were pooled from 5-8 plants per genetic background, for each independent experiment. Three repeats were performed. Whole leaves were placed in a petri dish abaxial side up in fresh opening buffer (OB) containing 10 mM MES, 20 µM $CaCl_2$, 50 mM KCl, and 1% sucrose at pH 6.15 for 3 hours under constant light. Leaves were then transferred to closing buffer (CB) containing 10 mM MES at pH 6.15 with 20 µM ABA. At indicated time points, abaxial epidermal strips were carefully peeled and imaged using a confocal microscope (Nikon Eclipse C90i). NIS-Elements software was used to manually determine the width of stomatal apertures at their widest point.

Confocal microscopy and quantification of filamentous actin (F-actin) variations in guard cells

Confocal microscopy was performed using a Nikon Eclipse C2plus system. Images were taken using intact leaves at room temperature with a Plan Flour 60x oil objective (numerical aperture of 1.4, excitation wavelength 488 nm, emission wavelength 516 nm). Six plants, grown under long-day conditions (16 hours light; 8 hours dark), were used for each genetic background, for each independent experiment. For each repeat, leaves were pooled from six plants, and three repeats were performed. Z-stacks were collected of the cortical layer of guard cells (ensuring exclusion of any nuclear signal) and used for subsequent quantification (Hwang and Lee, 2001; Eun et al., 2001; Gao et al., 2008). The number of filaments was quantified as described previously (Biel et al., 2020b, Biel et al., 2022).

Shoot biomass measurements

Arabidopsis thaliana WT and mutant seeds were germinated on soil in a humid chamber (with a lid) under a 16-hour light/8-hour dark regime. For long day biomass measurements, the lid was removed, and fresh weight of the rosette was measured once plants were 4 weeks old. For short day biomass measurements, the lid was removed, and the plants were transferred to a chamber with an 8-hour light/16-hour dark regime. Fresh weight of the rosette was measured once plants were 6 weeks old.

Root morphology assay

Arabidopsis thaliana WT and mutant seeds were germinated on Murashige and Skoog medium plates (Caisson Laboratories) lacking sucrose under constant light. At 12 days post-germination, images of seedlings were taken and root morphology was quantified using ImageJ.

Trichome branch number and length quantification

Rosette leaves from 3-week-old WT and mutant plants were imaged using a Nikon SMZ1270 Stereomicroscope using a 4X zoom. Branch number and length quantification were measured using ImageJ.

Trichome nuclear shape and size analysis

To visualize nuclei, trichomes were stained as previously described (Liang et al., 2019). Briefly, the third and fifth rosette leaves from 2-3 week old WT and mutant plants were used (clipped from seedlings on MS plates). At least five plants per genetic background were used, for three independent repeats of staining. Leaves were fixed in 3:1 ethanol/acetic acid for 2 hours at room temperature, washed for three times with distilled water (3x15 minutes), and stained by 3µg/mL of 4',6-Diamidino-2-phenylindole dihydrochloride (DAPI) for at least 30 minutes. Samples were mounted in immersion oil and imaged using a 40X oil objective on a Nikon Eclipse C2plus system. Circularity index and area of each nucleus were quantified using ImageJ. At least 45 trichomes were imaged and quantified per genetic background.

Alexa 488 Phalloidin trichome staining

The trichome actin cytoskeleton was visualized as previously described (Basu et al., 2005). Briefly, 2-3 week-old leaves were fixed in 4% formaldehyde in PEM buffer (100 mM Pipes-KOH, 5 mM EGTA, and 4 mM $MgCl_2$, pH 6.9) for 45 min. After two washes with PEM, the tissues were incubated in PEM containing 1% glycerol and 0.198 µM Alexa Fluor 488 phalloidin (Thermo Fisher Scientific, Cat. No. A12379) overnight at 4°C. Confocal microscopy was performed using a Nikon Eclipse C2plus system to visualize the actin cytoskeleton. Z-stacks were collected of the cortical layer and used for subsequent quantification. Ten plants were grown per genetic background for three rounds of staining and imaging, resulting in 21 trichomes imaged and quantified.

Occupancy quantification of phalloidin-stained trichomes

Occupancy was quantified as previously described (Higaki et al., 2010; Biel et al., 2022). Briefly, a maximum intensity projection was created from the acquired z-stacks. To perform noise reduction, a 1–5 pixel-band-pass filter was applied using the LPX Filter2d plugin (filter = bandpass; bpmode = Gaussian; lo = 1; hi = 5). The image was then binarized by thresholding. A region of interest (ROI) was drawn around the trichome stalk to determine the number of pixels occupied by actin filaments (GFP signal). Occupancy was calculated using the following formula: $occupancy\ (\%) = \frac{n_{GFP}}{n_{ROI}} \times 100$, where nGFP and nROI are the pixel numbers constituting the actin filaments and cell region of interest, respectively.

Results

Genetic Interaction between SINE1, SINE2, and Actin Remodeling Factors during Stomatal Closure

We have previously shown that the plant KASH proteins SINE1 and SINE2 are required for actin reorganization during ABA-induced stomatal closure (Biel et al., 2022). To investigate if SINE1 and SINE2 are playing this role, in conjunction with known guard cell actin organizers, we tested here stomatal closure and actin reorganization in the double mutants *arpc4-1 sine1-1*, *arpc4-1 sine2-1*, *scab1-2 sine1-1*, and *scab1-2 sine2-1* (see Materials and Methods).

Reduction of stomatal aperture was measured for 180 minutes after application of 20 μM ABA (Figure 1). WT stomatal apertures had closed from 4.5 μm to 2.5 μm after 180 minutes, similar to previous studies (Biel et al., 2020a). Delayed stomatal closure in response to both ABA and H_2O_2 has been previously reported in *arpc4-1* (Li et al., 2014). Here, we show that *arpc4-1* stomata closed to about 3.5 μm after 3 hours, similar to *sine1-1,* and consistent with the previously reported *sine1-1* defect (Figure 1A, Biel et al., 2020a). Interestingly, *arpc4-1 sine1-1* closed to the same extent as the single mutants, indicating no additive effect on the closing defect. Similarly, *sine2-1* and *arpc4-1* displayed identical closing defects at all timepoints, and the *arpc4-1 sine2-1* double mutant behaved in the same manner (Figure 1B). These data suggest that, in the context of stomatal closure, SINE1 and SINE2 act in the same complex or pathway as the ARP2/3 complex.

During ABA-induced stomatal closure, the *scab1-2* single mutant displays a delayed closure, rather than the inability to fully close in the time window of the assay (Zhao et al.,

2011). Thus at 120 minutes post-ABA treatment, *scab1-2* apertures were less closed than WT, but more closed than *sine1-1* (Figure 1C). At 180 minutes post-ABA treatment, *scab1-2* apertures were closed at a similar level to WT. At 120 minutes, the *scab1-2 sine1-1* mutant closely resembled *scab1-2* (Figure 1C). However, at 180 min, unlike *scab1-2*, the double mutant failed to close completely. This complex pattern could be interpreted as *SCAB1* being epistatic to *SINE1* up to 120 minutes of ABA treatment. After that time, *SINE1* appears epistatic to *SCAB1*. In contrast, the *scab1-2 sine2-1* double mutant had a similar stomatal closure defect to that of *sine2-1*, suggesting that *SINE2* is epistatic to SCAB1 throughout the assay (Figure 1D). Thus, loss of SCAB1 partially rescues the stomatal closure defect of *sine1-1* through an activity in the first 120 minutes of the assay but has no influence on *sine2-1*.

Interaction of SINE1, SINE2, and ARPC4 in ABA-induced actin reorganization

Next, actin reorganization during ABA-induced stomatal closure in each genetic background was observed, using 35S promoter-driven GFP-LIFEACT as an actin marker (Tolmie et al., 2017; Biel et al., 2022). Actin reorganization during stomatal closure, as visualized by this marker, has been previously reported for *sine1-1* and *sine2-1* (Biel et al. 2022). GFP-LIFEACT was introduced into the remaining genetic backgrounds, including the single and double mutants of *arpc4-1* and *scab1-2*, as well as the double mutant *sine1-1 sine2-1*. Introduction of the GFP-LIFEACT marker did not impact ABA-induced stomatal closure in WT, or any of the *sine, arpc4, or scab1* mutant backgrounds (Supplemental Figure 1).

Actin reorganization was observed over 120 minutes after application of ABA, as previously described (Biel et al. 2022). In WT stomata, actin filaments were arrayed in a radial pattern when in an open configuration (Fig 2A, 0 min; Biel et al., 2022). Following exposure to ABA, actin depolymerized as stomatal closure progressed (Figure 2A, 60 min). Finally, actin

repolymerized into bundled, longitudinal filaments, as stomata entered a closed state (Figure 2A, 120 min; Biel et al., 2022). We quantified the actin dynamics during stomatal closure using an actin classification previously described (Biel et al., 2022). Guard cells with radially arranged F-actin, with filaments extending from the dorsal to ventral guard cell walls, were classified as type 1. Guard cells with diffuse or mixed (radial and longitudinal) filaments were classified as type 2; with predominantly diffuse signal and fragmented F-actin subclassified as type 2a, and predominately mixed filaments with little or no diffuse signal subclassified as type 2b. Guard cells with longitudinally bundled actin cables were classified as type 3.

As previously reported, *sine1-1* stomata displayed an actin repolymerization defect, in which radially arrayed actin filaments depolymerized, but largely failed to repolymerize by 120 minutes (compare type 2a and type 3) (Figure 2A, 2B; Biel et al., 2022). In *sine2-1* stomata, filaments did not depolymerize to the degree seen in WT (compare types 2a and 2b) and remained a mixture of radial and longitudinal filaments. Actin reorganization failed to recover to the predominantly longitudinal state observed in WT (compare types 2b and 3) (Figure 2A, 2B; Biel et al., 2022). In addition, the *sine1-1 sine2-1* double mutant displayed actin depolymerization defects similar to *sine2-1,* consistent with the hypothesis that SINE2 acts at an earlier depolymerization stage and SINE1 at a later repolymerization stage (Supplemental Figure 2).

As previously described, the number of filaments was determined by the number of fluorescent peaks along the mid-width line of each guard cell (Li et al., 2014; Biel et al., 2022). Open WT guard cells had significantly more filaments than *sine1-1*, *sine2-1*, and *sine1-1 sine2-1* (0 min, Figure 2G, Figure S2D). During ABA-induced stomatal closure, the number of filaments decreased significantly in WT (Figure 2G, Figure S2D; Biel et al., 2022). Compared to WT, the

number of filaments decreased less in *sine1-1*, *sine2-1*, and *sine1-1 sine2-1* (Figure 2G, Figure S2D).

In *arpc4-1* stomata, guard cell actin was largely radially arrayed at 0 min, and filaments were mostly depolymerized by 60 min (Figure 2C, 2D). Similar to *sine1-1*, actin remained largely depolymerized at 120 min, compared to the longitudinal filaments observed in WT (compare type 2a and 3) (Figure 2C, 2D; Jiang et al., 2012; Biel et al., 2022). While the actin patterning at 0 min in *arpc4-1* was similar to WT, fewer filaments were present, similar to *sine1-1* (Figure 2G, 2H). At 60 min and 120 min, the filament number in both *sine1-1* and *arpc4-1* was consistent with WT levels. The *arpc4-1 sine1-1* double mutant mirrors the defect in repolymerization observed in the *sine1-1* and *arpc4-1* mutants (Figure 2C, 2D). Consistent with the actin organization data, the filament number in *arpc4-1 sine1-1* mirrors the single mutants at every time point (Figure 2H).

The distribution of actin patterns in *arpc4-1 sine2-1* is intermediary between *sine2-1* (little depolymerization, randomly organized filaments) and *arpc4-1* (no repolymerization at 120 minutes). Interestingly, *arpc4-1* can thus somewhat rescue the depolymerization defect in *sine2-1*, while *sine1-1* cannot (Figure 2D). Taken together, these data indicate that SINE1 and the ARP2/3 complex are involved in the same pathway during stomatal actin reorganization, while SINE2 and the ARP2/3 complex have opposing effects.

Loss of SCAB1 leads to a delay in actin reorganization, rather than an arrest (Zhao et al., 2011). At 120 min, the portion of type 3 actin is decreased compared to WT (Figure 2A, 2E, 2F, 2I). This correlates with the stomatal aperture measurements in Figure 1, where at 120 min, *scab1-2* apertures are more open than in WT, but at 180 min, they are closed to the same degree (Figure 1C-D; Zhao et al., 2011). At 180 minutes, the portion of type 3 actin in *scab1-2* increases

to similar levels as WT, and consistent with the stomatal closure data (Figure 1C, Supplemental Figure 3A, 3C). In the *scab1-2 sine1-1* double mutant, actin organization mirrors the *scab1-2* mutant through 120 min (Figure 2E, 2F, 2I). Interestingly, the *scab1-2 sine1-1* double mutant does not exhibit the actin repolymerization defect that *sine1-1* displays. The actin organization in *scab1-2* and *scab1-2 sine1-1* mirrors the stomatal aperture measurements, where at 120 min, *scab1-2* is identical to *scab1-2 sine1-1* (Figure 1C). This is consistent with the above interpretation that *SCAB1* is epistatic to *SINE1* up to 120 minutes of ABA treatment. At 180 minutes, the *scab1-2 sine1-1* double mutant maintains a large proportion of type 2A actin observed at 120 minutes, and only a marginal increase in type 3 actin (Supplemental Figure 3A, 3B). This is again consistent with the stomatal closure data. Indeed, there is little change in the actin organization pattern of *scab1-2 sine1-1* between 120 minutes and 180 minutes (compare Figure 2F with Supplemental Fig 3A), consistent with *sine1-1* being epistatic to *scab1-2* during this latter part of the assay.

In the *scab1-2 sine2-1* double mutant, an actin depolymerization defect similar to *sine2-1* is observed (Figure 2E, 2F, 2I). This is consistent with the stomatal aperture measurements, where both *sine2-1* and *scab1-2 sine2-1* stomata fail to close after 180 min (Figure 1D). This indicates that *SINE2* is also epistatic to *SCAB1* at the level of actin filament reorganization, in close correlation to the data shown in Figure 1.

***Arpc4-1 sine1-1* plants have vegetative growth defects**

Under long-day conditions, no vegetative growth defects were observed in *sine1-1*, *sine2-1*, or *arpc4-1* (Figure 3). In the *arpc4-1 sine1-1* double mutant, plants had smaller rosettes compared to WT and single mutant plants and an over 50% reduction in fresh weight at 4 weeks of growth, while *arpc4-1 sine2-1* grew WT-like (Figure 3A - 3C). Similarly, under short day

conditions, *arpc4-1 sine1-1* plants had smaller rosettes compared to WT and single mutants, while *arpc4-1 sine2-1* did not (Figure 3D). When quantified, an even more severe reduction in fresh weight compared to long day growth conditions was observed in *arpc4-1 sine1-1*, but not *arpc4-1 sine2-1*, compared to WT (Figure 3E, 3F). Under both long-day and short-day conditions, *sine1-1* and *arpc4-1* single mutants had no substantial growth defects (Figure 3B, 3E). The fresh weight of *sine2-1* was increased compared to WT under long day conditions (Figure 3C). In summary, the combination of the *arpc4-1* allele with the *sine1-1* allele led to a substantial reduction of shoot biomass in both long-day and short-day conditions, while *sine2-1* had no such effect.

A defect in pavement cell lobe length in *arpc4-1* has previously been reported (Li et al., 2003). To determine if the *arpc4-1 sine* double mutants had any leaf patterning defects, pavement cell morphology was imaged and measured (Supplemental Figure 4A-4D). No differences in pavement cell neck width were observed in *sine1-1*, *sine2-1*, *arpc4-1*, or any of the associated double mutants (Supplemental Figure 4C). The *arpc4-1 sine1-1* and *arpc4-1 sine2-1* double mutants, showed a similar reduction in lobe length as *arpc4-1*, indicating that SINE1 and SINE2 play no additional role in pavement cell morphology (Supplemental Figure 4D).

Because the *sine1-1 sine2-1* double mutant has an effect on lateral root growth (Biel et al., 2020a) and the ARP2/3 complex is expressed in the root tip and root vasculature (García-González et al., 2020), we also tested seedling root development (Figure 4A). The single mutants *sine1-1* and *aprc4-1* had no effect on primary root length, lateral root number, and lateral root density (Figure 4B – 4D). In contrast, primary root length was reduced to a small, but statistically significant, degree in *arpc4-1 sine1-1* (Figure 4B). More apparent was the reduction of lateral roots in *arpc4-1 sine1-1* compared to WT and the single mutants, leading also to a

reduced density of lateral roots (Figure 4C, 4D). Similar to the shoot growth phenotype, no differences were observed in root development in *sine2-1* and the *arpc4-1 sine2-1* double mutant (Figure 4E-4G).

Loss of SINE2 renders trichome development independent of ARP2/3

The ARP2/3 complex has previously been reported to be required for trichome branching (Li et al., 2003; Mathur et al., 2003b; Saedler et al., 2004). Because SINE2 (but not SINE1) is expressed in trichomes and the SINE2 protein is associated with the trichome nucleus (Zhou et al., 2014), we also assessed whether *sine2-1* had an influence on the known *arpc4-1* trichome phenotypes (Kotchoni et al., 2009). *arpc4-1* trichomes have a branching defect that results in stunted, asymmetrical trichome branches while *sine2-1* trichomes are WT-like (Figure 5A, 5C; Kotchoni et al., 2009). Interestingly, loss of SINE2 partially rescued the *arpc4-1* defect, resulting in elongated, symmetrical branches in the double mutant (Figure 5A, 5D). While there is a small reduction in branch number in *arpc4-1* trichomes (Figure 5B), the predominant phenotype lies in the strongly reduced length of the second and third trichome branch (Figure 5D). In *arpc4-1 sine2-1,* the branch number is increased, with more trichomes showing four branches and a few even five branches (Figure 5B). Branch length is almost recovered to WT levels for all branches (Figure 5D). These data indicate that in the absence of SINE2, trichome branch elongation becomes independent of the ARP2/3 complex.

One hypothesis to explain this observation is that in the absence of SINE2 - shown to lead to more stabilized actin filaments in guard cells - an aspect of actin filament dynamics dependent on ARP2/3 is not required for trichome branch elongation. To probe into this hypothesis, we tested whether an obvious difference in the overall organization of F-actin could be observed in the double mutant trichomes. F-actin was visualized in mature trichomes by

staining with phalloidin because it has been shown that in *arp2-1* and *arp3-1* mutants, actin structural defects were detected in young as well as mature trichomes (Li et al., 2003). We focused on the trichome stalk because in ARP2/3 mutants transverse actin cables, instead of fine filaments, were detected in the trichome stalk (Li et al., 2003).

The actin cytoskeleton was clearly visualized in WT, and a similar actin organization was observed in *sine2-1* (Figure 6A). In contrast, *arpc4-1* and *arpc4-1 sine2-1* trichomes showed more bundled actin in both stalk and branches. This was confirmed by occupancy measurement, a quantitative assessment of filament bundling (Higaki et al., 2010, Higaki et al., 2017). While *sine2-1* is WT-like, a reduction in occupancy was measured for *arpc4-1* (Figure 6B). This reduction is consistent with the decrease in the amount of filamentous actin and an increase in bundled actin. Occupancy in the double mutant was still reduced compared to WT and *sine2-1* and statistically indistinguishable from *arpc4-1* (Figure 6B). This suggests that the increase in filament bundling caused by *arpc4-1* is, at least in the stalk of mature trichomes, not rescued by the loss of SINE2.

To address other possible causes for the rescue, we investigated shape and size of the trichome nucleus. It has been shown that the number of trichome branches is closely correlated with nuclear DNA content (Tominaga-Wada et al., 2011; Yang and Ye, 2013, Liang et al., 2019). While the effect of ARP2/3 mutants on the trichome nucleus has not been investigated, it was shown for the trichome branching mutant *spike1-7* that the nucleus has an altered position compared to WT (Liang et al., 2019). SINE2 is a nuclear envelope KASH protein, and similar plant proteins have been shown to affect nuclear shape (Zhou et al., 2012; Zhou et al., 2015).

Therefore, we determined the total area of the mature trichome nucleus imaged after DAPI staining as well as a circularity index (4π[area/perimeter^2]). In WT, trichome nuclei were

elongated or spindle shaped (Figure 6D). Nuclei in *sine2-1* mutants were indistinguishable from WT for both nuclear area and circularity (Figure 6C, 6D). In contrast, *arpc4-1* nuclei were both smaller and more circular than WT, suggesting an effect of the ARP2/3 complex on trichome nuclear morphology. In the *arpc4-1 sine2-1* trichomes, the elongated nuclear shape was to a large degree restored, however the nuclear area remained as small as in *arpc4-1*. This indicates that *sine2-1* rescued the nuclear shape defect observed in *arpc4-1*. In none of the mutants was there a difference in the ratio of nuclei found in the stalk or the branch, suggesting that neither ARPC4 nor SINE2 affect nuclear positioning in mature trichomes (Supplemental Fig 5).

Discussion

After the discovery of SINE1 and SINE2 we had hypothesized that only SINE1 has a guard-cell-related function (Zhou et al., 2014). This was based on three lines of reasoning. (1) In leaves, SINE1 is specifically expressed in the guard cell lineage. (2) Only in *sine1-1* are the typically paired guard cell nuclei positioned more randomly. (3) Only the SINE1 ARM domain co-localizes in guard cells with F-actin. However, when probing into the guard cell physiology of *SINE1* and *SINE2* loss-of function mutants we found that both affected stomatal dynamics, and in many cases in the same ways. However, some differences were also observed, importantly a different interaction of the two mutants with actin-modulating drugs (Biel et al., 2020a). Follow-up research showed that actin remodeling in guard cells is disrupted in both *sine1-1* and *sine2-1*, but that the defects occurred at different stages of actin reorganization (Biel et al., 2022). Loss of SINE1 impaired the ability of actin to re-form filaments during reorganization and/or

maintain a polymerized state while loss of SINE2 impaired the ability of filamentous actin (F-actin) to depolymerize (Biel et al., 2022).

While ABA-induced stomatal closing in the *sine1-1 sine2-1* double mutant is similar to that in the *sine1-1* and *sine2-1* single mutants (Biel et al., 2020a), how actin organization is affected in the double mutant had not been investigated. Here, we show that ABA-induced actin reorganization in *sine1-1 sine2-1* resembles that of *sine2-1*, with a mixed F-actin pattern throughout ABA-induced stomatal closure, and little to no depolymerization or reorganization. This suggests that *sine2-1* is epistatic to *sine1-1*, consistent with the notion that SINE2 acts at an earlier depolymerization stage and thus upstream of SINE1.

As reported previously, a mutation in one of the subunits of the ARP2/3 complex disrupted ABA-induced closure similarly to *sine1-1* and *sine2-1* (Jiang et al., 2012; Biel et al., 2020a). We therefore asked whether combining loss of function of the ARP2/3 complex with loss of function of either SINE1 or SINE2 would lead to additive or synergistic defects in actin reorganization during stomatal closure. Stomatal closure was inhibited to the same degree in *sine1-1* and *arpc4-1* and in the double mutant and *arpc4-1* and *arpc4-1 sine1-1* displayed an actin reorganization defect similar to *sine1-1*. Together, this suggests that SINE1 and the ARP2/3 complex are involved in the same process. While inhibition in closing was also indistinguishable in the *sine2-1*, *arpc4-1*, and *sine2-1 arpc4-1* double mutant, the actin pattern in *arpc4-1 sine2-1* was intermediary between *sine2-1* and *arpc4-1*. This suggests that the additional loss of the ARP2/3 complex function can partially overcome the lack of actin depolymerization observed in *sine2-1*. This in turn suggests that SINE2 and the ARP2/3 complex play opposite roles during

actin reorganization, with SINE2 functioning in filament depolymerization and ARP2/3 in filament extension.

The data is consistent with a role for SINE1 and SINE2 as positive and negative regulators of ARP2/3, respectively. If and how such an activity is realized in guard cells, and if it is related to the nuclear envelope association of SINE1 and SINE2 will have to be addressed. It has been demonstrated that the plant ARP2/3 complex, like its animal counterpart, produces branched actin filaments at a branching angle of 70º (Cifrova et al., 2020). It can thus be assumed that such a network, and its dynamic changes, are in action during stomatal aperture regulation. Interestingly, the ARPC2 subunit of the Arabidopsis ARP2/3 complex also binds to microtubules (Havelkova et al., 2015). Given that in *sine1* and *sine2* mutants, microtubule organization is also affected during stomatal closure (Biel et al., 2020b), this is another potential avenue for future exploration of the functional interaction of a plant LINC complex with the ARP2/3 complex.

SCAB1 is an unusual actin-remodeling protein in that it is both plant- and guard-cell specific. It was shown to bundle and stabilize F-actin and to regulate the rearrangement of F-actin in guard cells during ABA-induced stomatal closure (Zhao et al., 2011; Zhang et al., 2013; Yang et al., 2021). The interaction between SCAB1 and SINE1 and SINE2 in guard cells is complex. It could be interpreted as *SCAB1* being epistatic to *SINE1* up to 120 minutes of ABA treatment, but *SINE1* being epistatic to *SCAB1* during the latter part of closing, while *SINE2* is epistatic to *SCAB1* throughout the assay. Thus, loss of SCAB1 partially rescues the stomatal closure defect induced in *sine1-1* through an activity in the first 120 minutes of the assay but has no influence on *sine2-1*. At 180 minutes, loss of SINE1 and SCAB1 results in an inability to repolymerize, and consequently fails to completely close the stomatal pore (Figure 1C,

Supplemental Figure 3). Compared to the *sine1-1* mutant, the *scab1-2 sine1-1* mutant loses the delayed ability to bundle actin and close stomata, observed in *scab1-2*, confirming SINE1 is epistatic to SCAB1 also in terms of actin organization during the latter stage of the assay and suggesting a role for SINE1 in actin bundling, too.

Interestingly, a reduced number of lateral roots was observed in *arpc4-1 sine1-1*, but not in *arpc4-1 sine2-1*, although SINE1 and SINE2 are both expressed in seedling roots. In Arabidopsis, LRs are formed from founder cells in the pericycle opposite to the xylem poles (Péret et al., 2009; Vermeer and Geldner, 2015). During lateral root initiation, a pair of adjacent founder cells expand radially and their nuclei migrate toward the common cell wall, followed by an asymmetric, anticlinal cell division giving rise to two shorter daughter cells at the center (Vilches Barro et al., 2019). The actin cytoskeleton has been shown to play a crucial role in LR initiation, specifically for the polar migration of the nucleus in the founder cells (Vilches Barro et al., 2019). Treatment with Latrunculin B led to a loss of coordinated nuclear migration in founder cells, resulting in symmetric divisions and aberrant lateral root formation (Vilches Barro et al., 2019). It is thus tempting to speculate that loss of SINE1 exaggerates the loss of the ARP2/3 complex for an F-actin remodeling step required for nuclear movement prior to asymmetric cell division, because (as seen in guard cells) both lead to reduced actin filament growth. Loss of SINE2, on the other hand, might antagonize the loss of ARP2/3 and thus not affect asymmetric founder cell division.

Previous studies have shown that loss of the ARP2/3 complex leads to aberrant trichome branching due to defects in actin organization (Li et al., 2003; Mathur et al., 2003b; Saedler et al., 2004). We show here that the additional absence of SINE2 rescues the ARP2/3 complex branch elongation phenotype. This suggests that trichome branch elongation becomes

independent of the ARP2/3 complex when SINE2 is also absent. However, the increase in filament bundling caused by *arpc4-1* was, at least in the stalk of mature trichomes, not rescued by the loss of SINE2. Nuclear shape was also perturbed in *arpc4-1*, where nuclei were round compared to elongated nuclei observed in WT. Interestingly, *arpc4-1 sine2-1* trichome nuclei were more elongated than *arpc4-1* trichome nuclei. In contrast, reduction in nuclear size, a second *arpc4-1* phenotype, appears to be independent of the presence or absence of SINE2. Thus, the ARP2/3 complex may be required for a connection of the trichome nucleus to the cytoskeleton in the presence of SINE2. In the absence of SINE2, however, nuclear shape becomes independent of the ARP2/3 complex.

One possible explanation is that other forces are then able to re-connect the nucleus to the cytoskeleton and lead to its elongation in the absence of SINE2. While this interpretation might be oversimplified, the data show a tight correlation between nuclear shape (and, by extension, attachment to actin filaments) and trichome branch elongation. It is thus possible that an elongated, and therefore F-actin-connected nucleus is required for an unknown signaling step important for the orchestration of branch elongation.

Together, our data show strong further evidence that the molecular roles of both SINE1 and SINE2 relate to the regulation of F-actin remodeling. While previously only observed in guard cells, the double mutant combinations examined here now also reveal roles in trichome and lateral root development and an effect on overall plant fitness. An interesting question for further investigation is how the specific genetic interactions of either SINE1 or SINE2 with the known actin-remodeling activities relate to their molecular roles.

We currently do not know how the cellular functions of SINE1 and SINE2 relate to their association with the nuclear envelope. Perinuclear F-actin has been visualized by PALM

microscopy in plant cells (Durst et al., 2014). In addition, tobacco ARP3 has been visualized at the sites of F-actin nucleation, including the nuclear periphery (Maisch et al. 2009). In dendritic cells, the ARP2/3 complex has been implicated in organizing an F-actin cage around the nucleus that disrupts the nuclear lamina, thus reducing nuclear stiffness and allowing for increased cell migration through tight spaces (Thiam et al., 2016). It is therefore conceivable that in guard cells and the other plant tissues investigated here, an aspect of actin remodeling is initiated by protein complexes at the nuclear envelope, involving SINE1 and SINE2. Probing into the requirement of the nuclear envelope associated C-terminal domain of SINE1 and SINE2 for the now-revealed spectrum of cellular and organismal functions will be one approach to further address this question.

Acknowledgments

We thank all members of the Meier lab for fruitful discussions throughout this work and Ms. Katelyn Amstutz for critical reading of the manuscript.

Author Contributions

IM, NRG, and MM designed the experiments. MM performed and analyzed the experiments. MM, NRG, and IM wrote and edited the manuscript and IM provided oversight and funding for the study.

Conflict of Interest

The authors declare no conflicts of interest.

Funding

This work was funded by a National Science Foundation grant to I.M. (NSF-2023348).

Data Availability

All original data files will be made available upon request.

References

Basu, D., Le, J., El-Essal, S., Huang, S., Zhang, C., Mallery, E. L., Koliantz, G., Staiger, C. J., Szymanski, D. B. (2005). DISTORTED3/SCAR2 is a putative Arabidopsis WAVE complex subunit that activates the Arp2/3 complex and is required for epidermal morphogenesis. *The Plant Cell* 17, 502-524.

Biel, A., Moser, M., Meier, I. (2020a). A Role for Plant KASH Proteins in Regulating Stomatal Dynamics. *Plant Physiol*ogy 182, 1100-1113.

Biel, A., Moser, M., Meier, I. (2020b). Arabidopsis KASH proteins SINE1 and SINE2 are involved in microtubule reorganization during ABA-induced stomatal closure. *Frontiers in Plant Science* 11, 575573.

Biel, A., Moser, M., Groves, N. R., Meier, I. (2022). Distinct roles for KASH proteins SINE1 and SINE2 in guard cell actin reorganization, calcium oscillations, and vacuolar remodeling. *Frontiers in Plant Science* 13, 784342.

Cifrova, P., Oulehlova, D., Kollarova, E., Martinek, J., Rosero, A., Zarsky, V., Schwarzerova, K., Cvrckova, F. (2020). Division of Labor Between Two Actin Nucleators – the Formin FH1 and the ARP2/3 Complex – in *Arabidopsis* Epidermal Cell Morphogenesis. *Frontiers in Plant Science* 11, 148.

Coates, J. C. (2003). Armadillo repeat proteins: beyond the animal kingdom. *Trends in Cell Biology* 13, 463-471

Dittmer, T. A., Stacey, N. J., Sugimoto-Shirasu K., Richards E. J. (2007). LITTLE NUCLEI Genes Affecting Nuclear Morphology in *Arabidopsis thaliana*. *The Plant Cell* 19, 2793-2803

Durst A., Hedde P. N., Brochhausen, L., Nick, P., Nienhaus, G. U., Maisch, J. (2014). Organization of perinuclear actin in live tobacco cells observed by PALM with optical sectioning. *Journal of Plant Physiology* 171, 97-108

Eun, S. O., Bae, S. H., and Lee, Y. (2001). Cortical actin filaments in guard cells respond differently to abscisic acid in wild-type and abi1-1 mutant Arabidopsis. *Planta* 212, 466-469.

Gao, X. Q., Chen, J., Wei, P. C., Ren, F., Chen, J., Wang, X. C. (2008). Array and distribution of actin filaments in guard cells contribute to the determination of stomatal aperture. *Plant Cell Reports* 27, 1655-1665.

Garcia-Gonzalez, J., Kobrlova, S., Semerak, M., Lacek, J., Baby, I. K., Petrasek, S., Schwarzerova, K. (2020). Arp2/3 complex is required for auxin-driven cell expansion through regulation of auxin transporter homeostasis. *Frontiers in Plant Science* 11, 486.

Goley, E. D., Rammohan, A., Znameroski, E. A., Firat-Karalar, E. N., Sept, D., Welch, M. D. (2010). An actin-filament-binding interface on the Arp2/3 complex is critical for

nucleation and branch stability. *Proceedings of the National Academy of Sciences, USA* 107, 8159-8164.

Goley, E. D., and Welch, M. D. (2006). The ARP2/3 complex: an actin nucleator comes of age. *Nature Reviews Molecular Cell Biology* 7, 713-726.

Goto, C., Tamura, K., Fukao, Y., Shimada, T., Hara-Nishimura, I. (2014). The Novel Nuclear Envelope Protein KAKU4 Modulates Nuclear Morphology in *Arabidopsis*. *The Plant Cell* 26, 2143-2155.

Gournier, H., Goley, E. D., Niederstrasser, H., Trinh, T., Welch, M. D. (2001). Reconstitution of Human Arp2/3 Complex Reveals Critical Roles of Individual Subunits in Complex Structure and Activity. *Molecular Cell* 8, 1041-1052.

Havelkova, L., Nanda, G., Martinek, J., Bellinvia, E., Sikorova, L., Slajcherova, K., Seifertova, D., Fischer, L., Fiserova, J., Petrasek, J., Schwarzerova, K. (2015). Arp2/3 complex subunit ARPC2 binds to microtubules. *Plant Science* 241, 96-108

Higaki, T. (2017). Quantitative evaluation of cytoskeletal organizations by microscopic image analysis. *Plant Morphology* 29, 15-21.

Higaki, T., Katsuna, N., Sano, T., Kondo, N., Hasezawa, S. (2010). Quantification and cluster analysis of actin cytoskeletal structures in plant cells: role of actin bundling in stomatal movement during diurnal cycles in Arabidopsis guard cells. *The Plant Journal* 61, 156-165.

Hwang, J. U., and Lee, Y. (2001). Abscisic acid-induced actin reorganization in guard cells of dayflower is mediated by cytosolic calcium levels and by protein kinase and protein phosphatase activities. *Plant Physiology* 125, 2120-2128.

Ivakov, A., and Persson, S. (2013). Plant cell shape: modulators and measurements. *Frontiers in Plant Science* 4, 439.

Jiang, K., Sorefan, K., Deeks, M. J., Bevan, M. W., Hussey, P. J., and Hetherington, A. M. (2012). The ARP2/3 Complex Mediates Guard Cell Actin Reorganization and Stomatal Movement in *Arabidopsis*. *The Plant Cell* 24, 2031-2040.

Kim, M., Hepler, P. H., Eun, S.-O., Ha, K. S., Lee, Y. (1995). Actin filaments in mature guard cells are radially distributed and involved in Stomatal movement. *Plant Physiology* 109, 1077-1084.

Kotchoni, S.O., Zakharova, T., Mallery, E.L., Le, J., El-Assal, S.E.-D., and Szymanski, D.B. (2009). The Association of the Arabidopsis Actin-Related Protein2/3 Complex with Cell Membranes Is Linked to Its Assembly Status But Not Its Activation. *Plant Physiology* 151, 2095-2109.

Li, S., Blanchoin, L., Yang, Z., Lord, E. M. (2003). The Putative Arabidopsis Arp2/3 Complex Controls Leaf Cell Morphogenesis. *Plant Physiology* 132, 2034-2044.

Li, L.-J., Ren, F., Gao, X.-Q., Wei, P.-C., Wang, X.-C. (2012). The reorganization of actin filaments is required for vacuolar fusion of guard cells during stomatal opening in *Arabidopsis*. *Plant Cell and Environment* 36, 484-497.

Li, X., Li, J.-H., Wang, W., Chen, N.-Z., Ma, T.-S., Xi, Y.-N., Zhang, X.-L., Lin, H.-F., Yang, B., Huang, S.-J., Chen, Y.-L. (2014). ARP2/3 complex-mediated actin dynamics is required for hydrogen peroxide-induced stomatal closure in *Arabidopsis*. *Plant Cell and Environment* 37, 1548-1560.

Liang, S., Yang, X., Deng, M., Zhao, J., Shao, J., Qi, Y., Liu, X., Yu, F., An, L. (2019). A New Allele of the *SPIKE1* Locus Reveals Distinct Regulation of Trichome and Pavement Cell Development and Plant Growth. *Frontiers in Plant Science* 10, 16.

Maisch, J., Fiserova, J., Fischer, L., Nick, P. (2009). Tobacco Arp3 is localized to actin-nucleating sites *in vivo*. *Journal of Experimental Botany* 60, 603-614

Mathur, J., Mathur, N., Kernebeck, B., and Hülskamp, M. (2003a). Mutations in actin-related proteins 2 and 3 affect cell shape development in Arabidopsis. *The Plant Cell* 15, 1632-1645.

Mathur, J., Mathur, N., Kirik, V., Kernebeck, B., Srinivas, B. P., Hülskamp, M. (2003b). *Arabidopsis CROOKED* encodes for the smallest subunit of the ARP2/3 complex and controls cell shape by region specific fine F-actin formation. *Development* 130, 3137-3146.

Meier, I., Richards, E. J., and Evans D. E. (2017). Cell Biology of the Plant Nucleus. *Annual Review of Plant Biology* 68, 139-172.

Péret, B., De Rybel, B., Casimiro, I., Benková, E., Swarup, R., Laplaze, L., Beeckman, T., and Bennett, M. J. (2009). Arabidopsis lateral root development: an emerging story. *Trends in Plant Science* 14, 399-408.

Poulet, A., Probst, A. V., Graumann, K., Tatout, C., Evans D. E. (2017). Exploring the evolution of the proteins of the plant nuclear envelope. *Nucleus* 8, 46-59.

Saedler, R., Mathur, N., Srinivas, B. P., Kernebeck, B., Hülskamp, M., Mathur, J. (2004). Actin Control Over Microtubules Suggested by *DISTORTED2* Encoding the *Arabidopsis* ARPC2 Subunit Homolog. *Plant Cell Physiology* 45, 813-822

Sahi, V. P., Cifrová, P., García-González, J., Kotannal Baby, I., Mouillé, G., Gineau, E., Müller, K., Baluška, F., Soukup, A., Petrášek, J., Schwarzerová, K. (2018). Arabidopsis thaliana plants lacking the ARP2/3 complex show defects in cell wall assembly and auxin distribution. *Annals of Botany* 122, 777-789.

Starr, D. A., and Fridolfsson, H. N. (2010). Interactions between nuclei and the cytoskeleton are mediated by SUN-KASH nuclear-envelope bridges. *Annual Review of Cell and Developmental Biology* 26, 421-444.

Tamura, K., Iwabuchi K., Fukao Y., Kondo M., Okamoto, K., Ueda, H., Nishimura, M., Hara-Nishimura, I. (2013). Myosin XI-I Links the Nuclear Membrane to the Cytoskeleton to Control Nuclear Movement and Shape in *Arabidopsis*. *Current Biology* 23, 1-6.

Thiam, H.-R., Vargas, P., Carpi, N., Crespo, C. L., Raab, M., Terriac, E., King, M. C., Jacobelli, J., Alberts, A. S., Stradal, T., Lennon-Dumenil, A.-M., Piel, M. (2016). Perinuclear Arp2/3-driven actin polymerization enables nuclear deformation to facilitate cell migration through complex environments. *Nature Communications* 7, 10997

Tolmie, F., Poulet, A., McKenna, J., Sassmann, S., Graumann, K., Deeks, M., Runions, J. (2017). The cell wall of *Arabidopsis thaliana* influences actin network dynamics. *Journal of Experimental Botany* 68, 4517-4527.

Vermeer, J. E. M., and Geldner, N. (2015). Lateral root initiation in *Arabidopsis thaliana*: a force awakens. *F1000Prime Reports* 3, 7-32

Vilches Barro, A., Stockle, D., Thellmann, M., Ruiz-Duarte, P., Bald, L., Louveaux, M., von Born, P., Denninger, P., Goh, T., Fukaki, H., Vermeer, J. E. M., Maizel, A. (2019). Cytoskeletal Dynamics Are Necessary for Early Events of Lateral Root Initiation in *Arabidopsis*. *Current Biology* 29, 2443-2454.

Winter, D., Vinegar, B., Nahal, H., Ammar, R., Wilson, G. V., Provart N. J. (2007). An "Electronic Fluorescent Pictograph" Browser for Exploring and Analyzing Large-Scale Biological Data Sets. *PLoS One* 2, e718.

Xiao, Y., Chen, Y., Huang, R., Chen, J., and Wang, X.-C. (2004). Depolymerization of actin cytoskeleton is involved in stomatal closure-induced by extracellular calmodulin in Arabidopsis. *Science in China Series C: Life Sciences* 47, 454-460.

Yang, Y., Zhao, Y., Zheng, W., Zhao, Y., Zhao, S., Wang, Q., Bai, L., Zhang, T., Huang, S., Song, C., Yuan, M., Guo, Y. (2021). Phosphatidylinositol 3-phosphate regulates SCAB1-mediated F-actin reorganization during stomatal closure in Arabidopsis. *The Plant Cell* 34, 477-494.

Zhang, C., Mallery, E. L., Szymanski, D. B. (2013). ARP2/3 localization in Arabidopsis leaf pavement cells: a diversity of intracellular pools and cytoskeletal interactions. *Frontiers in Plant Science* 4, 1-16.

Zhang, X., Dyachok, J., Krishnakumar, S., Smith, L. G., Oppenheimer, D. G. (2005). *IRREGULAR TRICHOME BRANCH* in Arabidopsis Encodes a Plant Homolog of the Actin-Related Protein 2/3 Complex Activator SCAR/WAVE That Regulates Actin and Microtubule Organization. *The Plant Cell* 17, 2314-2326

Zhao, S., Jiang, Y., Zhao, Y., Huang, S., Yuan, M., Zhao, Y. (2016). CASEIN KINASE1-LIKE PROTEIN2 regulates actin filament stability and stomatal closure via phosphorylation of actin depolymerizing factor. *The Plant Cell* 28, 1422-1439.

Zhao, Y., Zhao, S., Mao, T., Qu, X., Cao, W., Zhang, L., Zhang, W., He, L., Li, S., Ren, S., Zhao, J., Zhu, G., Huang, S., Ye, K., Yuan, M., Guo, Y. (2011). The Plant-Specific Actin Binding Protein SCAB1 Stabilizes Actin Filaments and Regulates Stomatal Movement in *Arabidopsis*. *The Plant Cell* 23, 2314-2330.

Zhou, X., Graumann, K., Evans, D. E., Meier, I. (2012). Novel plant SUN-KASH bridges are involved in RanGAP anchoring and nuclear shape determination. *Journal of Cell Biology* 196, 203-211.

Zhou, X., Graumann, K., Wirthmueller, L., Jones, J. D. G., Meier, I. (2014). Identification of unique SUN-interacting nuclear envelope proteins with diverse functions in plants. *Journal of Cell Biology* 205, 677-692.

Zhou, X., Groves, N. R., Meier, I. (2015). Plant nuclear shape is independently determined by the SUN-WIP-WIT2-Myosin XI-I complex and CRWN1. *Nucleus* 6, 144-53.

Figure Legends

Figure 1. Genetic interactions between SINE proteins and known actin remodeling factors SCAB1 and ARP2/3 during ABA-induced stomatal closure.

ABA-induced stomatal closure assays were performed, and stomatal apertures were measured at 0, 60, 120, and 180 minutes after ABA exposure. (A) ABA-induced stomatal closure in *sine1* and *arpc4* mutants. (B) ABA-induced stomatal closure in *sine2* and *arpc4* mutants. (C) ABA-induced stomatal closure in *sine1* and *scab1* mutants. (D) ABA-induced stomatal closure in *sine1* and *scab1* mutants. Symbols in (A) and (B) denote statistical significance as determined by Student's *t* test, with $P < 0.05$. *Specified lines versus WT; °specified lines versus *sine1-1* or *sine2-1*; ¥ specified lines versus *arpc4-1*; ǂ specified lines versus *arpc4-1 sine1-1* or *arpc4-1 sine2-1*. Symbols in (C) and (D) denote statistical significance as determined by Student's *t* test, with $P < 0.05$. *Specified lines versus WT; °specified lines versus *sine1-1* or *sine2-1*; ¥ specified lines versus *scab1-2*; ǂ specified lines versus *scab1-2 sine1-1* or *scab1-2 sine2-1*. Error bars represent standard error. $N > 200$ for all data points.

Figure 2. Actin reorganization during ABA-induced stomatal closure.

ABA-induced stomatal closure assays were performed on plants expressing GFP-LIFEACT. (A) Representative images of actin patterning at 0, 60, and 120 minutes following addition of ABA, in WT and *sine* mutants. (B) Actin type analysis at 0, 60, and 120 minutes after addition of ABA, in WT and *sine* mutants. (C) Representative images of actin patterning at 0, 60, and 120 minutes following addition of ABA, in *arpc4* mutants. (D) Actin type analysis at 0, 60, and 120 minutes after addition of ABA, in *arpc4* mutants. (E) Representative images of actin patterning at 0, 60, and 120 minutes following addition of ABA, in *scab1* mutants. (F) Actin type analysis at 0, 60, and 120 minutes after addition of ABA, in *scab1* mutants. Actin filament number at 0, 60, and 120 minutes after ABA addition in WT and *sine* mutants (G), WT and *arpc4* mutants (H), and WT and *scab1* mutants (I). Filament numbers were determined from the images collected for data in panels B, D and F. Therefore, WT data are identical in panels G, H, and I, which have been separated to improve clarity. All images are maximum intensity projections of Z-stacks. Scale bar = 5 µM. $N \geq 50$ guard cells for each time point. All data are mean values ± SE from three independent experiments. Data collection included data shown in Supplemental Figures 1 and 2. Symbols denote statistical significance as determined by Student's *t* test compared to WT: *$P < 0.05$; ** $P < 0.01$; ***$P < 0.001$. Error bars are standard error.

Figure 3. Shoot growth phenotypes in *arpc4 and sine* mutants

(A) Representative images of 4-week-old plants grown in long day (16h light, 8h dark) for WT, *sine1-1*, *sine2-1*, *arpc4-1*, *arpc4-1 sine1-1*, and *arpc4-1 sine2-1*. Scale bar = 20 mm. (B) Fresh weight of *sine1* and *arpc4* mutants grown under long day (16h light, 8h dark) conditions after 4 weeks. (C) Fresh weight of *sine2* and *arpc4* mutants grown under long day (16h light, 8h dark) conditions after 4 weeks. (D) Representative images of 6-week-old plants grown in short day (8h light, 16h dark) for WT, *sine1-1*, *sine2-1*, *arpc4-1*, *arpc4-1 sine1-1*, and *arpc4-1 sine2-1*. Scale bar = 20 mm. (E) Fresh weight of *sine1* and *arpc4* mutants grown under short day (8h light, 16h

dark) conditions after 6 weeks. (F) Fresh weight of *sine2* and *arpc4* mutants grown under short day (8h light, 16h dark) conditions after 6 weeks. For all panels, N ≥ 20 plants per background per 3 biological repeats. Statistical significance was calculated using Student's *t* test. Lowercase letters denote groups that are statistically different ($p < 0.05$).

Figure 4. *arpc4 sine1-1* mutants have aberrant root morphology.

(A) Representative images of seedlings used for root morphology measurements. Scale bar = 0.5 cm. (B-D) Root morphology measurements of *sine1* and *arpc4* mutants. (E-G) Root morphology measurements of *sine2* and *arpc4* mutants. (B, E) Lateral root number. (C, F) Primary root length. (D, G) Lateral root density. Measurements were taken at 12 days post-germination. N ≥ 40 seedlings per background per biological repeat. Statistical significance was calculated using Student's *t* test. Lowercase letters denote groups that are statistically different ($p < 0.05$).

Figure 5. SINE2 and the ARP2/3 complex genetically interact in trichome morphology.

(A) Representative images of trichomes on a young leaf from WT, *sine2-1*, *arpc4-1*, and *arpc4-1 sine2-1* plants. Scale bar = 1 mm. (B) Quantitative analysis of the trichome branching phenotypes on the third and fifth rosette leaves of WT, *sine2-1*, *arpc4-1*, and *arpc4-1 sine2-1*. 2/3/4/5-br represented two/ three/ four/ five -branched trichomes, respectively. N = 213 trichomes from 3 biological repeats analyzed per background. (C) Single trichomes with branches from WT, *sine2-1*, *arpc4-1*, and *arpc4-1 sine2-1* plants. Scale bar = 100 µm. (D) Stalk and branch length of leaf trichomes of WT, *sine2-1*, *arpc4-1*, and *arpc4-1 sine2-1*. All data are mean values ± SE from three independent experiments. N = 105 trichomes from 3 biological repeats analyzed per background. Values in the bars indicate the number of trichomes that contained 3, 4, or 5 branches analyzed if under 105. Statistical significance was calculated using Student's *t* test. Lowercase letters denote groups that are statistically different within each category ($p < 0.05$).

Figure 6. SINE2 and the ARP2/3 complex influence nuclear shape, nuclear size, and actin patterning in trichomes.

(A) Representative images of WT, *sine2-1*, *arpc4-1*, and *arpc4-1 sine2-1* trichomes stained with Alexa Fluor 488 Phalloidin. All images are maximum intensity projections of Z-stacks. Scale bar = 50 µm. (B) Quantification of phalloidin-stained actin occupancy for WT, *sine2-1*, *arpc4-1*, and *arpc4-1 sine2-1*. N = 21 trichomes per background. (C) Representative images of WT, *sine2-1*, *arpc4-1*, and *arpc4-1 sine2-1* trichome nuclei stained with DAPI. Scale bar = 10 µm. Characteristics of DAPI-stained trichome nuclei were quantified with circularity index (D) and nuclear area (E). Statistical significance was calculated using Student's *t* test. Lowercase letters denote groups that are statistically different ($p < 0.05$). N = 45 trichome nuclei per background.

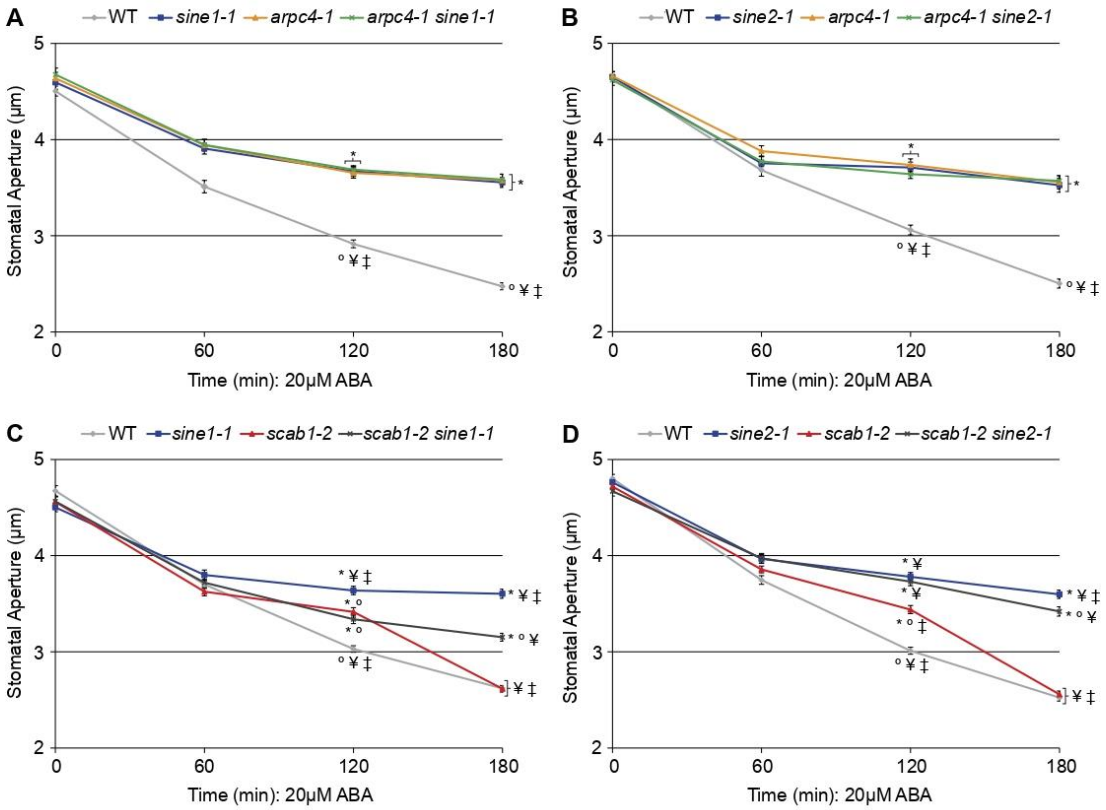

Figure 1. Genetic Interactions between SINE proteins and known actin remodeling factors SCAB1 and ARP2/3 during ABA-Induced Stomatal Closure.
ABA-induced stomatal closure assays were performed, and stomatal apertures were measured at 0, 60, 120, and 180 minutes after ABA exposure. **(A)** ABA-induced stomatal closure in *sine1* and *arpc4* mutants. **(B)** ABA-induced stomatal closure in *sine2* and *arpc4* mutants. **(C)** ABA-induced stomatal closure in *sine1* and *scab1* mutants. **(D)** ABA-induced stomatal closure in *sine1* and *scab1* mutants. Symbols in (A) and (B) denote statistical significance as determined by Student's *t* test, with $P < 0.05$. *Specified lines versus WT; °specified lines versus *sine1-1* or *sine2-1*; ¥ specified lines versus *arpc4-1*; ǂ specified lines versus *arpc4-1 sine1-1* or *arpc4-1 sine2-1*. Symbols in (C) and (D) denote statistical significance as determined by Student's *t* test, with $P < 0.05$. *Specified lines versus WT; °specified lines versus *sine1-1* or *sine2-1*; ¥ specified lines versus *scab1-2*; ǂ specified lines versus *scab1-2 sine1-1* or *scab1-2 sine2-1*. Error bars represent standard error. $N > 200$ for all data points.

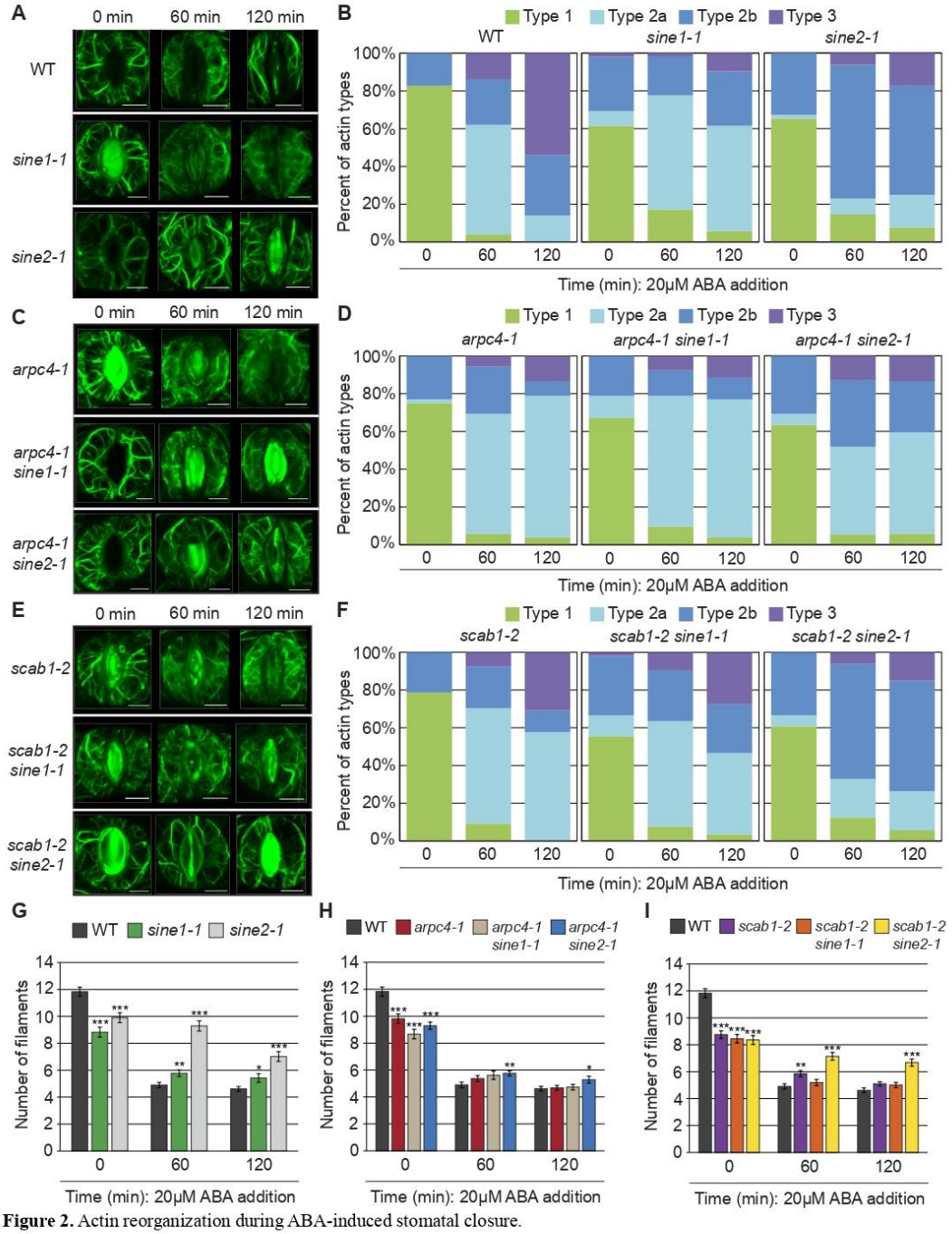

Figure 2. Actin reorganization during ABA-induced stomatal closure.
ABA-induced stomatal closure assays were performed on plants expressing GFP-LIFEACT. **(A)** Representative images of actin patterning at 0, 60, and 120 minutes following addition of ABA, in WT and *sine* mutants. **(B)** Actin type analysis at 0, 60, and 120 minutes after addition of ABA, in WT and *sine* mutants. **(C)** Representative images of actin patterning at 0, 60, and 120 minutes following addition of ABA, in *arpc4* mutants. **(D)** Actin type analysis at 0, 60, and 120 minutes after addition of ABA, in *arpc4* mutants. **(E)** Representative images of actin patterning at 0, 60, and 120 minutes following addition of ABA, in *scab1* mutants. **(F)** Actin type analysis at 0, 60, and 120 minutes after addition of ABA, in *scab1* mutants. Actin filament number at 0, 60, and 120 minutes after ABA addition in WT and *sine* mutants **(G)**, WT and *arpc4* mutants **(H)**, and WT and *scab1* mutants (I). All images are maximum intensity projections of Z-stacks. Scale bar = 5 μM. N ≥ 50 guard cells for each time point. All data are mean values ± SE from three independent experiments. Symbols denote statistical significance as determined by Student's *t* test compared to WT: *P < 0.05; ** P < 0.01; ***P < 0.001. Error bars are standard error.

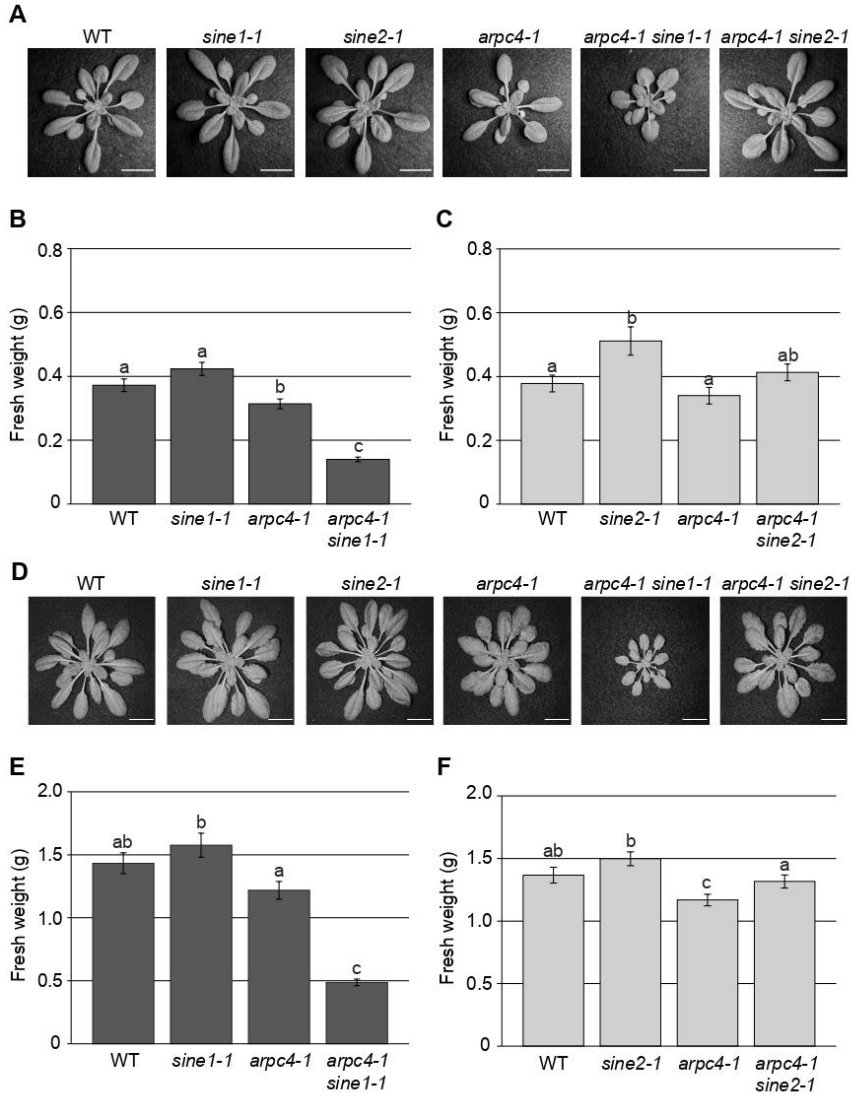

Figure 3. Shoot growth phenotypes in *arpc4* and *sine* mutants
(A) Representative images of 4-week-old plants grown in long day (16h light, 8h dark) for WT, *sine1-1*, *sine2-1*, *arpc4-1*, *arpc4-1 sine1-1*, and *arpc4-1 sine2-1*. Scale bar = 20 mm. **(B)** Fresh weight of *sine1* and *arpc4* mutants grown under long day (16h light, 8h dark) conditions after 4 weeks. **(C)** Fresh weight of *sine2* and *arpc4* mutants grown under long day (16h light, 8h dark) conditions after 4 weeks. **(D)** Representative images of 6-week-old plants grown in short day (8h light, 16h dark) for WT, *sine1-1*, *sine2-1*, *arpc4-1*, *arpc4-1 sine1-1*, and *arpc4-1 sine2-1*. Scale bar = 20 mm. **(E)** Fresh weight of *sine1* and *arpc4* mutants grown under short day (8h light, 16h dark) conditions after 6 weeks. **(F)** Fresh weight of *sine2* and *arpc4* mutants grown under short day (8h light, 16h dark) conditions after 6 weeks. For all panels, N ≥ 20 plants per background per 3 biological repeats. Statistical significance was calculated using Student's *t* test. Lower-case letters denote groups that are statistically different ($p < 0.05$).

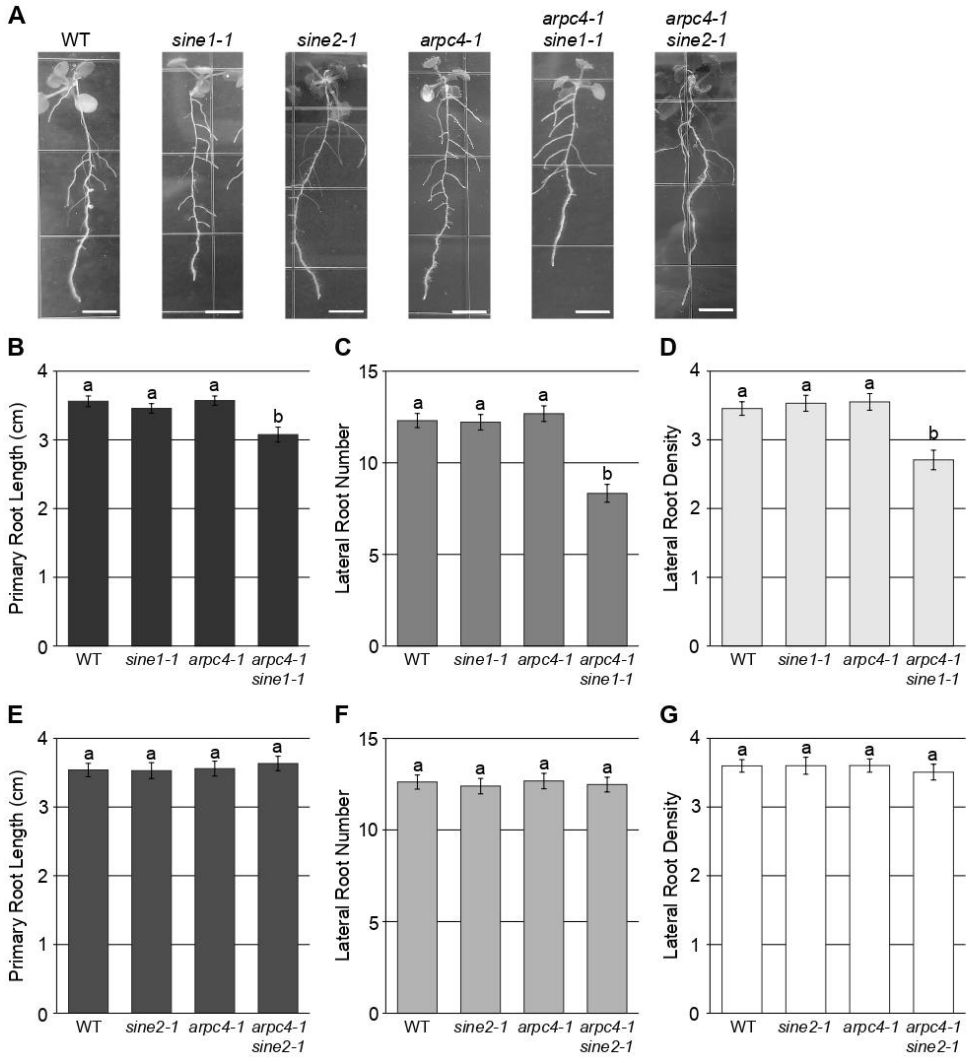

Figure 4. *arpc4 sine1-1* mutants have aberrant root morphology.
(A) Representative images of seedlings used for root morphology measurements. Scale bar = 0.5 cm. **(B-D)** Root morphology measurements of *sine1* and *arpc4* mutants. **(E-G)** Root morphology measurements of *sine2* and *arpc4* mutants. **(B, E)** Lateral root number. **(C, F)** Primary root length. **(D, G)** Lateral root density. Measurements were taken at 12 days post-germination. $N \geq 40$ seedlings per background per biological repeat. Statistical significance was calculated using Student's *t* test. Lowercase letters denote groups that are statistically different ($p < 0.05$).

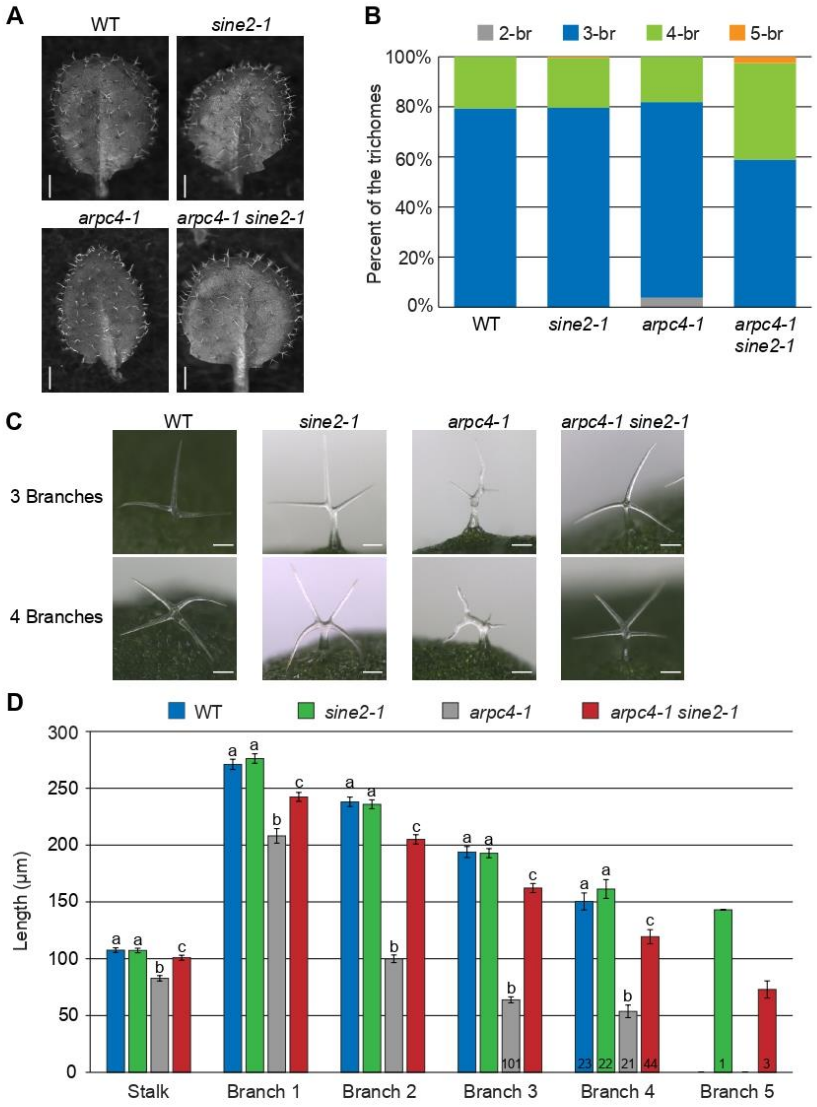

Figure 5. SINE2 and the ARP2/3 complex genetically interact in trichome morphology. **(A)** Representative images of trichomes on a young leaf from WT, *sine2-1*, *arpc4-1*, and *arpc4-1 sine2-1* plants. Scale bar = 1 mm. **(B)** Quantitative analysis of the trichome branching phenotypes on the third and fifth rosette leaves of WT, *sine2-1*, *arpc4-1*, and *arpc4-1 sine2-1*. 2/3/4/5-br represented two/ three/ four/ five -branched trichomes, respectively. N = 213 trichomes from 3 biological repeats analyzed per background. **(C)** Single trichomes with branches from WT, *sine2-1*, *arpc4-1*, and *arpc4-1 sine2-1* plants. Scale bar = 100 µm. **(D)** Stalk and branch length of leaf trichomes of WT, *sine2-1*, *arpc4-1*, and *arpc4-1 sine2-1*. All data are mean values ± SE from three independent experiments. N = 105 trichomes from 3 biological repeats analyzed per background. Values in the bars indicate the number of trichomes that contained 3, 4, or 5 branches analyzed if under 105. Statistical significance was calculated using Student's *t* test. Lowercase letters denote groups that are statistically different within each category ($p < 0.05$).

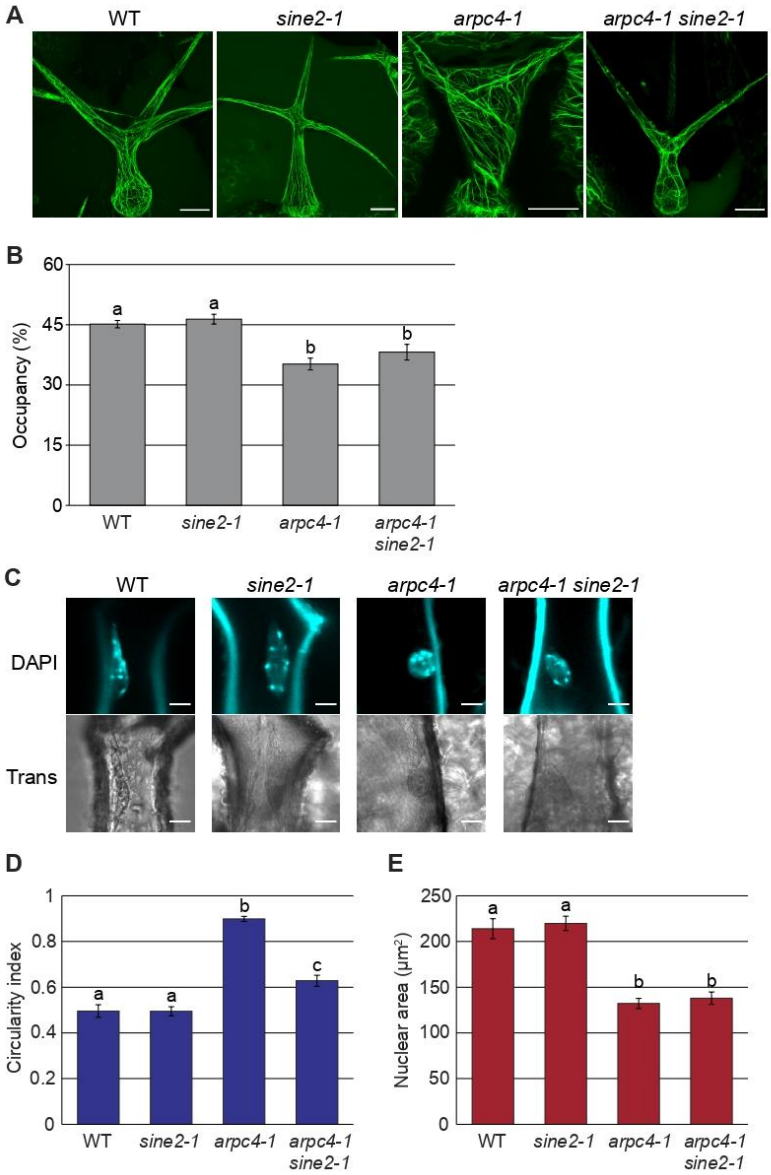

Figure 6. SINE2 and the ARP2/3 complex influence nuclear shape, nuclear size, and actin patterning in trichomes.
(A) Representative images of WT, *sine2-1*, *arpc4-1*, and *arpc4-1 sine2-1* trichomes stained with Alexa Fluor 488 Phalloidin. All images are maximum intensity projections of Z-stacks. Scale bar = 50 µm. **(B)** Quantification of phalloidin-stained actin occupancy for WT, *sine2-1*, *arpc4-1*, and *arpc4-1 sine2-1*. N = 21 trichomes per background. **(C)** Representative images of WT, *sine2-1*, *arpc4-1*, and *arpc4-1 sine2-1* trichome nuclei stained with DAPI. Scale bar = 10 µm. Characteristics of DAPI-stained trichome nuclei were quantified with circularity index **(D)** and nuclear area **(E)**. Statistical significance was calculated using Student's *t* test. Lowercase letters denote groups that are statistically different ($p < 0.05$). N = 45 trichome nuclei per background.